

PAPER

## Activation, decay heat, and waste classification studies of the European DEMO concept

To cite this article: M.R. Gilbert *et al* 2017 *Nucl. Fusion* **57** 046015

View the [article online](#) for updates and enhancements.

### Related content

- [European DEMO design strategy and consequences for materials](#)  
G. Federici, W. Biel, M.R. Gilbert et al.
- [An integrated model for materials in a fusion power plant: transmutation, gas production, and helium embrittlement under neutron irradiation](#)  
M.R. Gilbert, S.L. Dudarev, S. Zheng et al.
- [Materials-related issues in the safety and licensing of nuclear fusion facilities](#)  
N. Taylor, B. Merrill, L. Cadwallader et al.

# Activation, decay heat, and waste classification studies of the European DEMO concept

M.R. Gilbert<sup>1</sup>, T. Eade<sup>1</sup>, C. Bachmann<sup>2</sup>, U. Fischer<sup>3</sup> and N.P. Taylor<sup>1</sup>

<sup>1</sup> CCFE, Culham Science Centre, Abingdon, Oxfordshire, OX14 3DB, United Kingdom

<sup>2</sup> Eurofusion PMU, Boltzmannstr.2, Garching 85748, Germany

<sup>3</sup> Association KIT-Euratom, Karlsruhe Institute of Technology (KIT), Karlsruhe, Germany

E-mail: [mark.gilbert@ukaea.uk](mailto:mark.gilbert@ukaea.uk)

Received 22 September 2016, revised 9 January 2017

Accepted for publication 23 January 2017

Published 2 March 2017



CrossMark

## Abstract

Inventory calculations have a key role to play in designing future fusion power plants because, for a given irradiation field and material, they can predict the time evolution in chemical composition, activation, decay heat, gamma-dose, gas production, and even damage (dpa) dose. For conceptual designs of the European DEMO fusion reactor such calculations provide information about the neutron shielding requirements, maintenance schedules, and waste disposal prospects; thereby guiding future development.

Extensive neutron-transport and inventory calculations have been performed for a reference DEMO reactor model with four different tritium-breeding blanket concepts. The results have been used to chart the post-operation variation in activity and decay heat from different vessel components, demonstrating that the shielding performance of the different blanket concepts—for a given blanket thickness—varies significantly.

Detailed analyses of the simulated nuclide inventories for the vacuum vessel (VV) and divertor highlight the most dominant radionuclides, potentially suggesting how changes in material composition could help to reduce activity. Minor impurities in the raw composition of W used in divertor tiles, for example, are shown to produce undesirable long-lived radionuclides.

Finally, waste classifications, based on UK regulations, and a recycling potential limit, have been applied to estimate the time-evolution in waste masses for both the entire vessel (including blanket modules, VV, divertor, and some ex-vessel components) and individual components, and also to suggest when a particular component might be suitable for recycling. The results indicate that the large mass of the VV will not be classifiable as low level waste on the 100 year timescale, but the majority of the divertor will be, and that both components will be potentially recyclable within that time.

Keywords: fusion power plant concepts, neutron-induced transmutation and activation, DEMO designs, radioactive waste classification

(Some figures may appear in colour only in the online journal)

## 1. Introduction

During operation of a DEMOnstration fusion power plant, a large flux of 14 MeV neutrons will be generated within the burning plasma— $\sim 3.5 \times 10^{20}$  ns<sup>-1</sup> per GW of

deuterium-tritium (DT) fusion power—and these neutrons will necessarily impinge on the surrounding vessel components, causing structural damage and activation. The material activation, in particular, is problematic because the associated radiation fields (of  $\gamma$ -rays or photons, as well as  $\beta$  and  $\alpha$

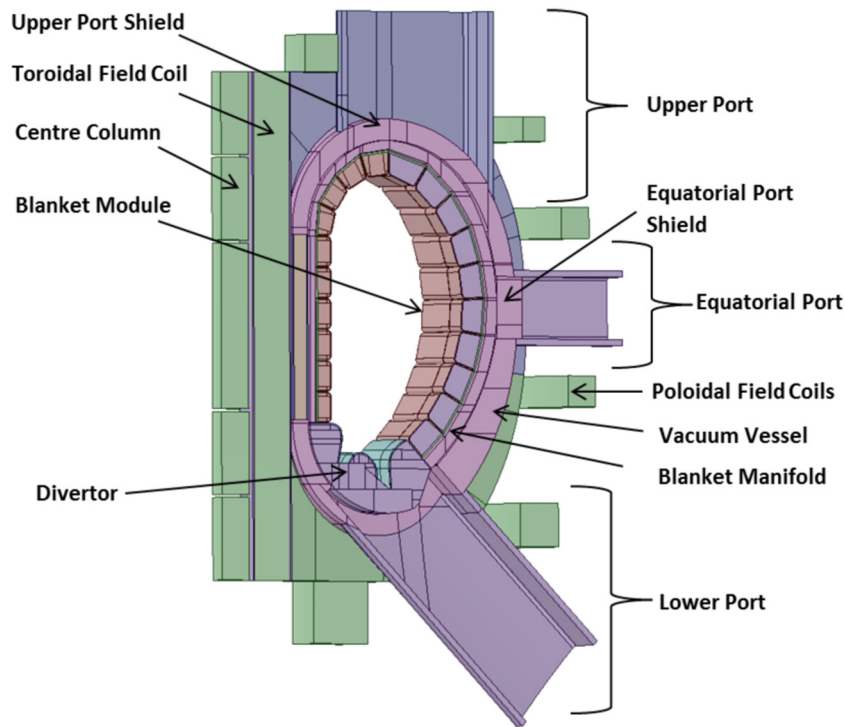


**Figure 1.** A schematic of the  $11.25^\circ$  sector DEMO model used for the neutron transport simulations.

particles) can severely hamper maintenance operations, and the cost of disposal and recycling prospects of waste at the end of reactor (or component) lifetime is one of the primary considerations when assessing the commercial viability of fusion power. Furthermore, the DT neutrons must be prevented from escaping or otherwise irradiating sensitive reactor components (such as electronics) or reactor personnel.

It is therefore important to perform analyses during the conceptual designing of DEMO to ensure that the shutdown activation (including decay heat to avoid expensive active cooling) and radioactive waste are minimised, and hence that there is sufficient neutron shielding within and surrounding the reactor vessel. Inventory calculations have a key role to play in this process because, for a given neutron irradiation field and material, they can predict the time evolution in composition, activation, decay heat,  $\gamma$ -dose, gas production, and even damage (dpa) dose. Combined with neutron transport calculations of DEMO designs (to define the neutron fields) such calculations can provide information about the neutron shielding requirements, possible maintenance schedules, and waste disposal prospects, thereby guiding future development.

The present paper describes calculations of post operation activation and decay heat of vessel components—the divertor and vacuum vessel (VV), in particular—as well as predictions of the build-up and evolution of different classifications of radioactive waste for the entire reactor model, and whether the waste is potentially recyclable. All of these are considered for a conceptual design of the European DEMO with four different tritium breeding blanket and cooling options, which allows for a basic analysis (in a fixed reactor geometry) of the likely implications of a particular choice on the activation

of components, and hence on the differing shielding performance and requirements of each option.

## 2. Calculations

The simulations and analyses presented here have three stages: (1) calculation of the neutron spectra and fluxes throughout the regions of interest in the DEMO geometry; (2) running of extensive inventory simulations (sometimes more than one) for each reactor region; and (3) post processing of the inventory results to define component-averaged results and/or waste classifications. The three steps are briefly described below before the presentation of the results in section 3.

### 2.1. 3D DEMO model and Monte Carlo neutron transport simulations

Neutron transport simulations have been performed using MCNPv6.1 [1] for a conceptual model of DEMO created within the European DEMO studies programme in 2014 (developed as part of [2], but see also, for example [3, 4]). The reactor symmetry makes it possible to model only an  $11.25^\circ$  sector of the full DEMO Tokamak with vertical reflecting planes at the  $0^\circ$  and  $11.25^\circ$  boundaries. The model has homogenized tritium blanket modules (i.e. containing no detailed structural features) whose thicknesses have nominally been optimised (for shielding and tritium-breeding-efficiency factors) to a helium-cooled pebble-bed blanket scenario.

Since DEMO is in the conceptual design phase, design changes of the breeding blanket can be expected in the future, e.g. in order to satisfy the tritium breeding requirement

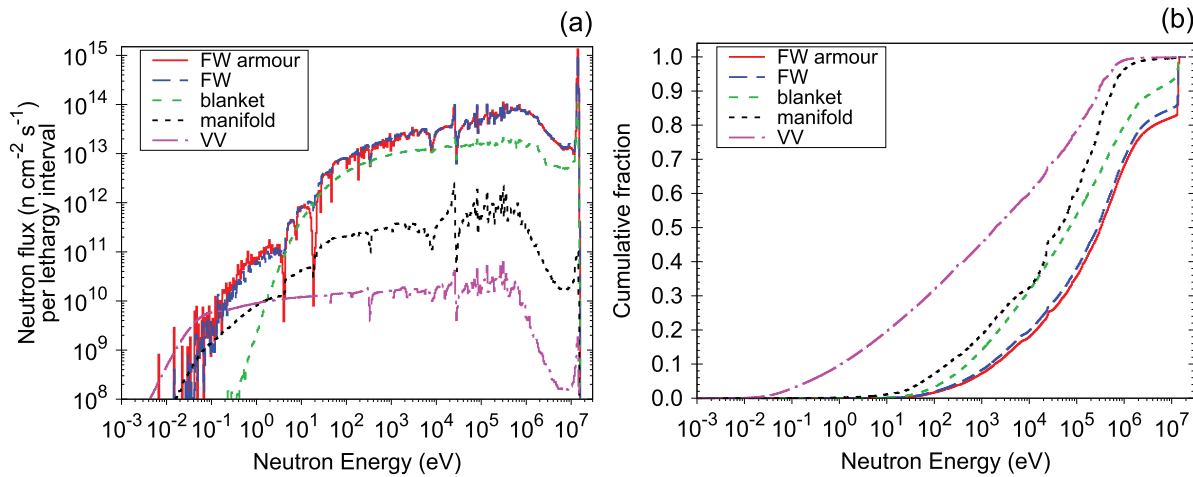


**Figure 2.** Neutron energy spectra simulated for the HCPB concept in different regions of the outboard equatorial first wall. (a) the absolute neutron fluxes per lethargy interval, and (b) normalised cumulative distributions. Note that these plots use a fine, 616 energy-bin structure [8] instead of the 175-group structure used for the inventory simulations.

(TBR > 1.05 [5]). However, here the main dimensions and material mixture of the breeding blanket are consolidated, see below, and hence the results obtained in this study are relevant and provide guidance in the further development of the DEMO design. In addition, the present case allows for a direct comparison of the relative shielding characteristics of the different concepts in identical geometric configurations. A schematic of the 3D-cell geometry of the DEMO design used within MCNP is shown in figure 1.

Four tritium-breeding concepts have been considered in this study by filling the blanket module cells with different material compositions at appropriate densities. These are (see [6] for more details):

- HCLL—a Helium-Cooled system with a liquid Lithium-Lead blanket (13% by volume EUROFER steel, 78% LiPb with 90% enrichment to  $^6\text{Li}$ , and 8% He at 80 bar pressure);
- HCPB—Helium-Cooled with a ceramic Pebble-Bed of beryllium and lithium-orthosilicate (11.8% EUROFER, 37.9% Be, 13%  $\text{Li}_4\text{SiO}_4$  with 60%  $^6\text{Li}$  enrichment, and a combination of He at 80 bar and 1 bar pressure totalling 37.3% of the volume in total);
- WCLL—Water-Cooled with liquid Lithium-Lead (18% EUROFER, 1.9% water, and 80.1% LiPb with 90%  $^6\text{Li}$  enrichment);
- DCLL—a Dual-Cooled reactor with a self-cooling liquid Lithium-Lead blanket and helium cooling elsewhere in the first wall, blanket cases, etc (12% EUROFER, 73% LiPb with 90%  $^6\text{Li}$  enrichment).

The volume % material compositions given in brackets above are for the homogenized blanket breeding modules themselves. In all cases the divertor is water cooled with a 5 mm tungsten plasma-facing layer (also used for the 2 mm first wall armour).

EUROFER is the primary in-vessel structural steel, with a wt.% composition of: 0.12% C, 0.6% Mn, 0.005% P, 0.005% S, 0.05% Si, 0.01% Ni, 9.5% Cr, 0.005% Mo, 0.24% V, 0.14% Ta, 1.2% W, 0.02% Ti, 0.01% Cu, 0.005% Nb, 0.01% Al,

0.045% N, 0.002% B, 0.01% Co, 0.01% As, 0.01% Sn, 0.01% Sb, 0.01% Zr, 0.01% O, and Fe the balance.

In other regions, including the vacuum vessel (VV) walls, SS316L(N)-IG is the primary steel, with a wt.% composition of: 0.03% C, 2% Mn, 0.5% Si, 0.025% P, 0.01% S, 18% Cr, 12.5% Ni, 2.7% Mo, 0.08% N, 0.001% B, 0.3% Cu, 0.05% Co, 0.01% Nb, 0.1% Ti, 0.01% Ta, and Fe the balance.

For each version of the model,  $10^9$  neutron histories were simulated in MCNP, which, combined with a neutron weight window generated using appropriate global variance reduction techniques [7], produced reasonable statistics (typically less than 5% uncertainty in total fluxes) for neutron spectra (in the standard 175-group Vitamin-J energy bin structure—see [8] for details) recorded in the cells (of which there are more than 800 in the present DEMO model) of interest. The nuclear interactions in the simulations were governed by the FENDL-2.1 [9] neutron-reaction cross section library, with supplementary information from the ENDF/B-VII.1 [10] library for nuclides that were absent from FENDL-2.1. Figure 2 shows some typical spectral results obtained, in this case for a series of locations at increasing depths into the outboard equatorial wall of the HCPB concept. The first wall (FW) armour is nearest to the plasma, followed by, in increasing depth order, FW, blanket, manifold, and VV. The full spectra in figure 2(a), which have been scaled from the ‘per-source-neutron’ results from MCNP to the 1.6 GW fusion power of the 2014 reactor concept (equivalent to  $\sim 5.6 \times 10^{20} \text{ ns}^{-1}$ ), illustrates the drop in total flux as the neutrons are gradually moderated and absorbed. Meanwhile, the normalised cumulative spectra in figure 2(b) show (more clearly than in figure 2(a)) how the neutron spectrum becomes increasingly moderated with depth—as neutrons under-go evermore interactions.

Figure 3, on the other hand, compares the spectrum for the same region of the DEMO model with the four different blanket concepts, in this case for the outboard equatorial VV wall. While the overall profile of the spectrum does not change with the four concepts (figure 3(b)), the absolute flux values (figure 3(a)) are significantly different. In particular, the fluxes experienced by the VV in the HCLL concept are around an

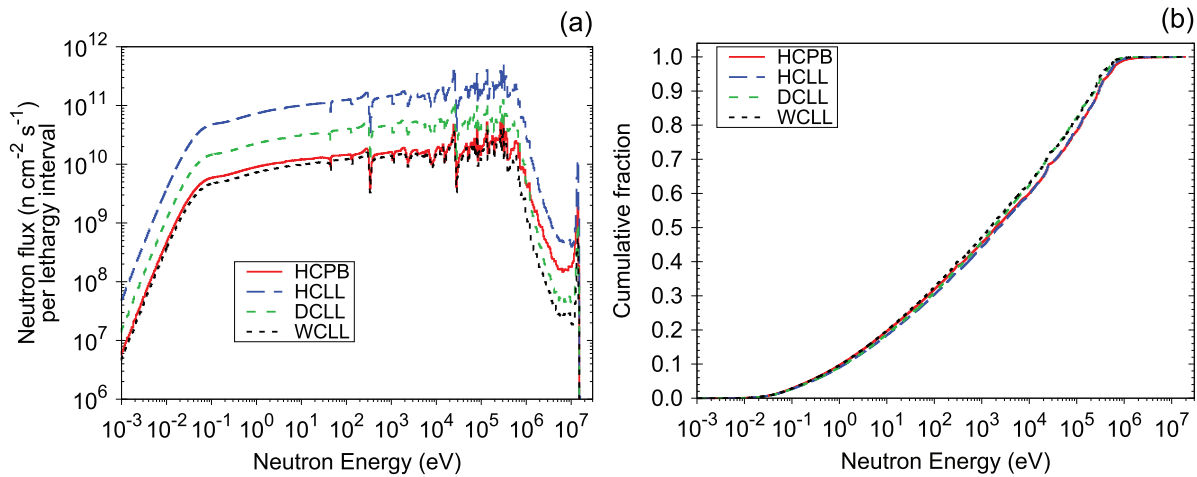


**Figure 3.** Neutron energy spectra simulated for the outboard equatorial vacuum vessel (VV) wall in the four different DEMO-blanket concepts. (a) the absolute neutron fluxes per lethargy interval, and (b) normalised cumulative distributions. Note that these plots use a fine, 616 energy-bin structure [8] instead of the 175-group structure used for the inventory simulations.

order of magnitude higher than those for the WCLL or HCPB concepts. This is in agreement with previous ‘DEMO comparison’ studies [11], where, in a somewhat different reactor geometry (an earlier concept within the European programme), it was again found that the neutron fluxes on the VV are highest behind the HCLL concept. Note that in that work [11] the HCLL concept was also predicted to have significantly higher fluxes in FW regions than HCPB (see figure 3 in [11]). The results presented later will show that this different shielding performance of the HCLL concept has significant implications on the activation of the VV.

## 2.2. Inventory simulations and processing

The neutron spectra tallies discussed above have been used in a sequence of detailed inventory simulations performed with the FISPACT-II [8] system using the EAF-2010 [12] neutron-reaction cross section library and associated decay data. The material in each non-empty cell (the geometry contains many vacuum cells) of the geometry was irradiated according to the full 2-phase operation scenario envisaged for DEMO [13] under the neutron spectrum predicted for that cell. Specifically, this involved a 5.2 year phase-1 period of pulsed operation (modelled in FISPACT-II in the standard way as a continuous flux at 30% of full power), followed by a 1 year shutdown for a complete blanket and divertor replacement, and then a further 14.8 year pulsed operation in phase 2, which was split into three parts (‘phases 2a–2c’) with 8 month shutdown periods for additional divertor replacements in between. Note that at the end of each phase the pulsed operation was modelled explicitly so as to accurately capture the short-lived radionuclides that might produce a significant radiological response immediately after shutdown.

The waste classification analyses performed in this work (see section 3.3) required further that additional inventory simulations be performed for the cells of the blanket and divertor, to match the number of times they are to be replaced—a removed component will still contribute to the overall waste

inventory. In practice, this meant two FISPACT-II simulations for each blanket cell: the first modelling the phase 1 irradiation and followed by a ‘zero-flux’ phase 2 schedule, which was required to have matching time-stepping to the end of DEMO lifetime in each file of FISPACT-II inventory results; and a second with only the phase 2 irradiation scenario (including divertor-replacement shutdowns). Similarly, four different simulations were required for each divertor cell—for phases 1, 2a–2c (again with blank, zero-flux time-steps as necessary to produce time-coherent results). All other cells were simulated once with both phase 1 and 2 included. At the end of the operational phase a sequence of decay-cooling steps were modelled to define activities at 1 s, 5 min, 30 min, 1 h, 3 h, 5 h, 10 h, 1 d, 2 d, 1 week, 2 weeks, 4 weeks, 8 weeks, 6 months, 1 year, 10 years, 100 years, and 1000 years after final DEMO shutdown.

The resulting set of FISPACT-II outputs (almost 1700 per DEMO-blanket concept) contains detailed nuclide inventory breakdowns as a function of concentration and radiological response, as well as total activities, decay-heats,  $\gamma$ -doses, inhalation and ingestion doses, and clearances indices, at each time-step (plasma-operation or shutdown). These outputs have been post-processed to extract and calculate relevant data, including total becquerel activity and decay heat (measured in watts), as well as contact  $\gamma$  dose rate (sievert per hour), which is needed to define the waste class of a particular cell (see section 3.3). Where appropriate, results have been summed or averaged as a function of reactor component, for example, over all cells of the VV, with a cell’s volume and density (from the MCNP model) used to define its mass scaling factor. Volumes were computed stochastically using a separate MCNP simulation, where the model is flooded with neutrons and all cells are set to vacuum so that the resulting cell tallies (with statistical uncertainties of less than 1%) define the pure volume fraction of the cell—i.e. without any nuclear reactions. Selected results, focusing in particular on comparisons between the four DEMO-blanket concepts, are presented in the following results section.

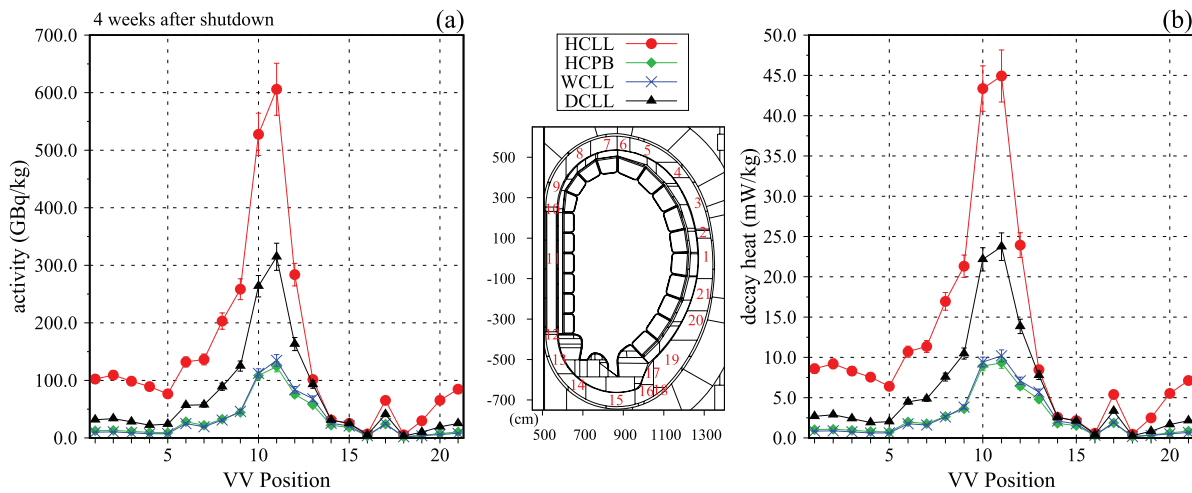


**Figure 4.** Poloidal variation in (a) total activity in  $\text{GBq kg}^{-1}$ , and (b) decay heat in  $\text{mW kg}^{-1}$ , of the VV four weeks after final DEMO shutdown. Results are shown for all four DEMO-blanket concepts. The toroidal cross section through the MCNP geometry indicates the position of the numbered VV cells in the plots. The error bars associated with each point in these plots (and elsewhere) are those computed by FISPACT-II based on the uncertainties in the input EAF-2010 [12] nuclear data.

### 3. Results

#### 3.1. Activity and decay heat

A direct application of the standard output from the inventory simulations is to analyze the poloidal variation in activity and decay heat at different decay-cooling times in the same component, illustrating the scope of the calculations and the level of detail available. Component averaging can then be used to look at the radiological responses as a function of time. The following results focus on the vacuum vessel (VV) and divertor.

**3.1.1. VV.** Figure 4 shows the poloidal variation in total activity and decay heat in the VV of the DEMO model with the four blanket concepts, four weeks after the final DEMO shutdown. The high level of activation in the relatively poorly shielded inboard equatorial VV regions is entirely expected as there is not much room for shielding, but the significantly higher result for VV regions behind the tritium breeding blanket of the HCLL concept is a potential cause for concern. This is caused by the higher neutron fluxes experienced by the HCLL-VV (see figure 3), and suggests that the HCLL (and to a lesser extent DCLL) concept would require relatively more shielding to protect the VV than either HCPB or WCLL, where the Be (HCPB) or water (WCLL) of their blanket modules greatly improves neutron moderation and absorption, and hence shielding. However, since the shielding and blanket design of the geometry used for these calculations was optimised for the HCPB concept, it may be that the effect here would be somewhat mitigated in a properly optimised configuration for each concept, without the need for any additional shielding.

Notice in figure 4 that the VV activation behind the divertor cassette at the bottom of the reactor (VV positions 13–18 in the figure) are virtually identical in the four blanket concepts, which is expected since the divertor cells do not differ. It is also important to remember here that the presented results in

the figure are for relatively large homogenised VV cells. This is particularly the case for the inboard VV. In a more heterogeneous model, for example with a VV made up of several layers, the activation results could be quite different. Such analyses are the subject of further studies [14], which will be presented in a future publication.

The relative comparison between the different cells of the VV does not change with time, so a plot of the situation after 10 years, for example, would look the same as figure 4, albeit with different absolute becquerel and watt scales. Thus, rather than considering more plots like this—showing the full poloidal variation,—it is instead more useful to examine the time-evolution. Figure 5 shows the time-evolution after shutdown in activity and decay heat per kg. The values shown are averages across the entire VV, where the mass of each cell was used to weight its contribution to the average. It demonstrates, on a logarithmic decay-timescale, that the activation of the material contained in the VV (predominantly a 80% SS316, 20% water by volume mix) falls by several orders of magnitude after only a few years. For example, the total activity per kg in the HCLL case drops from around 1 TBq immediately after shutdown to around 10 GBq after 10 years. As in figure 4, the activation of the VV behind HCLL blanket modules is the highest at all decay times, with the HCPB and WCLL concepts, in particular, producing almost an order of magnitude lower ‘per kg’ activities and decay heats at all times. It is interesting to note that the curves and data points for HCPB and WCLL in the figure are almost indistinguishable—in agreement with figure 4,—which is somewhat surprising given the different material compositions of the blanket modules that neutrons have been moderated by on their journey to the VV.

Using the full inventory output from FISPACT-II at each time-step, it is also possible to define the time-evolving nuclide contributions to the calculated total activity and decay heat. Figure 6 shows how the contributions from the most important radionuclides varies with time during decay-cooling for the VV of the HCLL concept (results for the other blanket

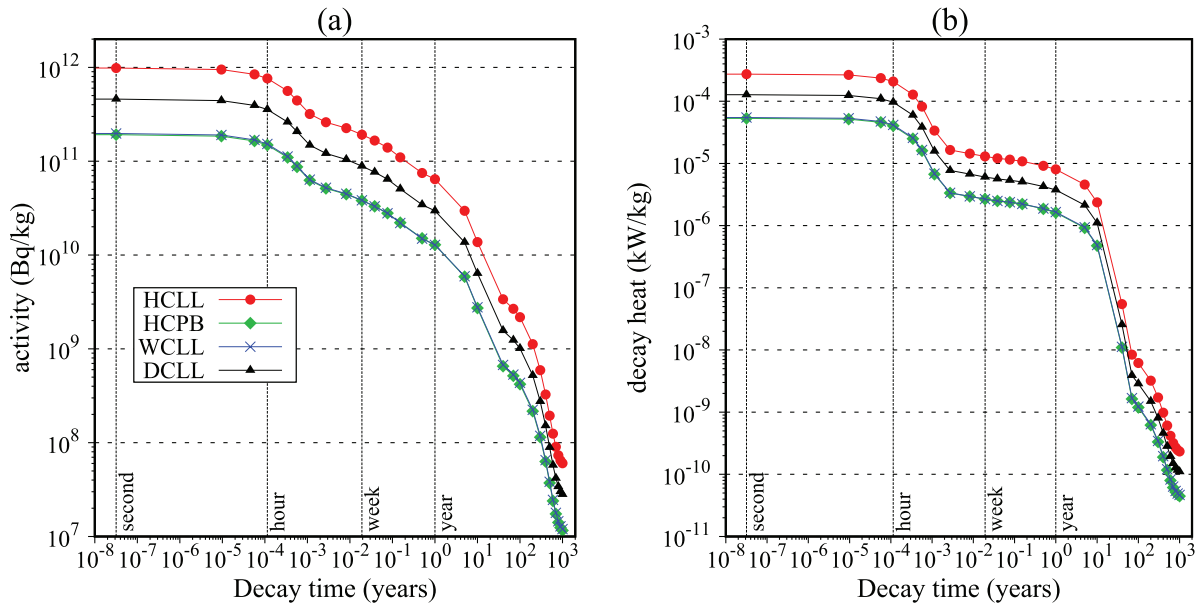


Figure 5. Decay profile of (a) activity, and (b) decay heat, averaged (by cell mass) across all VV cells.

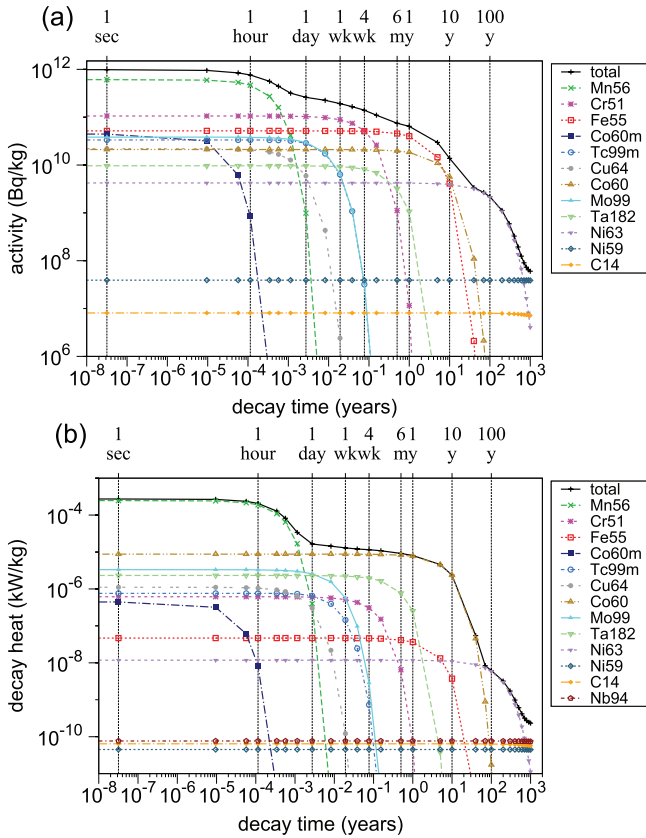


Figure 6. Radionuclide breakdown of the decay-profile of (a) activity, and (b) decay heat, averaged (by cell mass) across all VV cells of the HCLL concept.

concepts are similar but on different absolute scales)—again, mass-averaged across all VV cells.

For activity (figure 6(a)), it can be seen that at short time-scales the problematic (most dominant) radionuclide is  $^{56}\text{Mn}$  ( $T_{1/2} = 2.6\text{h}$ ), which is produced: at high neutron energies, from the main  $^{56}\text{Fe}$  isotope (91.8 atomic% of pure Fe, and

58.1 atm.% of SS316 overall) via (n,p)—neutron capture followed by proton emission—nuclear reactions; and at lower energies, via (n, $\gamma$ ) reactions on the 2 atm.% of  $^{55}\text{Mn}$  (100% of pure Mn) in the steel. At longer decay times, greater than 1 d, first  $^{51}\text{Cr}$  and then  $^{55}\text{Fe}$  become the most dominant nuclides, with half-lives of 27.7 d and 2.7 years, respectively. While  $^{55}\text{Fe}$  production is unavoidable (produced either from (n,2n) reactions on  $^{56}\text{Fe}$  or (n, $\gamma$ ) reactions on  $^{54}\text{Fe}$ ), the contribution from  $^{51}\text{Cr}$ , on the other hand, could be reduced if the concentration of Cr, responsible for the majority of its production, were lowered. Indeed, the reduced-activation EUROFER steel has significantly less Cr than SS316 (see section 2.1), and we shall see below in the divertor analysis that the  $^{51}\text{Cr}$  contribution is largely absent (figure 9).

Similarly, at very long decay times in figure 6(a)—greater than 10 years,—the dominant contribution from  $^{63}\text{Ni}$  ( $T_{1/2} = 100.6$  years) originates from the relatively high Ni content (12.5 wt.%) of SS316.

The decay heat radionuclide contributions in figure 6(b) are noticeably different to the activity results at medium time-scales between 1 d and 10 years. It is  $^{60}\text{Co}$  ( $T_{1/2} = 5.3$  years), instead of either  $^{55}\text{Fe}$  or  $^{51}\text{Cr}$ , that dominates the heat produced from the material because it is a significant  $\gamma$  emitter, while the other two predominantly decay via  $\beta$  emission, which does not produce as much heating.

**3.1.2. Divertor body.** In the DEMO model considered here the divertor is composed of three layers of cells: a plasma-facing armour layer of pure tungsten 5 mm thick; an intermediate layer, again dominated by W, but also containing CuCrZr, pure copper, and water to represent cooling channels; and then the bulk divertor body composed of EUROFER steel. Figure 7 shows a typical poloidal variation in the activity and decay-heat profiles for the different cells of the divertor body—in this case at 1 s after DEMO shutdown in the final replacement divertor. This ‘phase 2c’ divertor (see

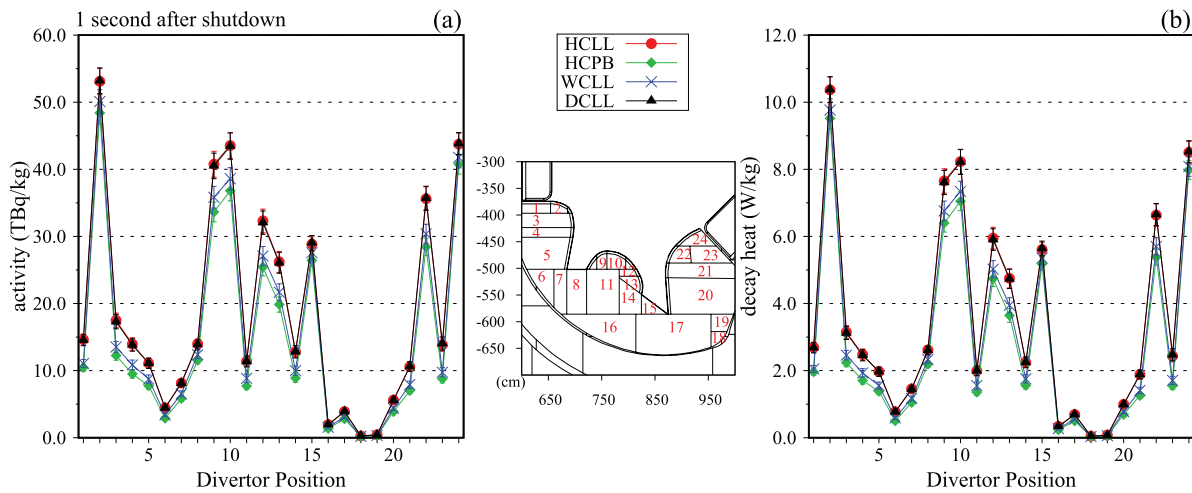


**Figure 7.** Poloidal variation in (a) total activity in  $\text{TBq kg}^{-1}$ , and (b) decay heat in  $\text{W kg}^{-1}$ , of the final replacement divertor body 1 s after DEMO shutdown. Results are shown for all four DEMO-blanket concepts. The toroidal cross section through the MCNP geometry indicates the position of the numbered divertor cells in the plots.

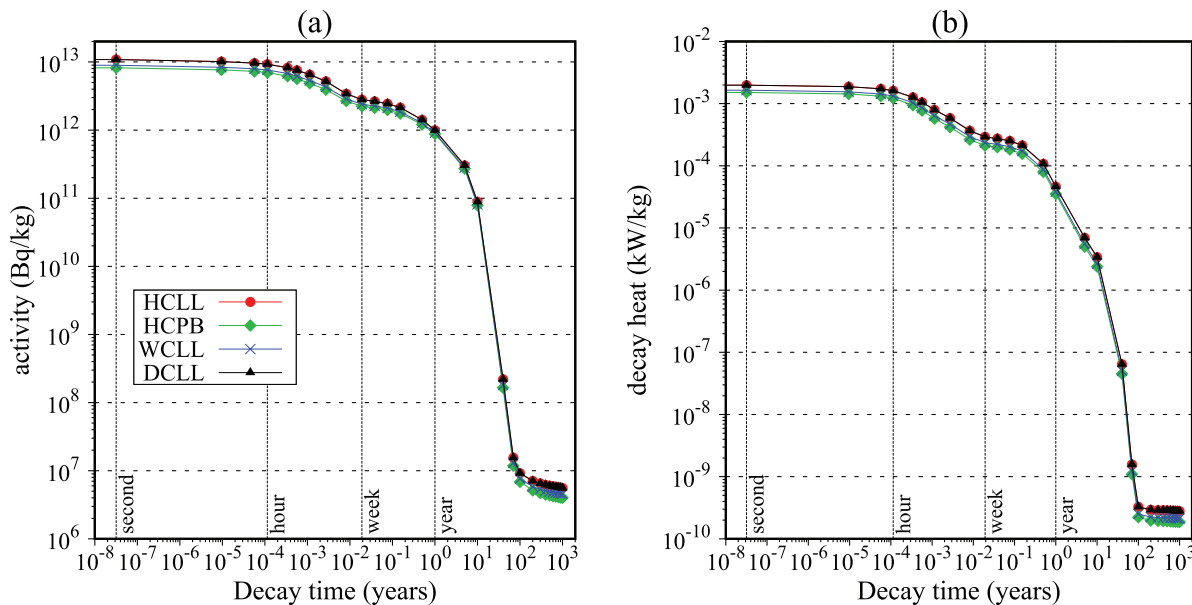


**Figure 8.** Decay profile of (a) activity, and (b) decay heat, averaged (by cell mass) across all divertor body cells (following irradiation of the final replacement divertor).

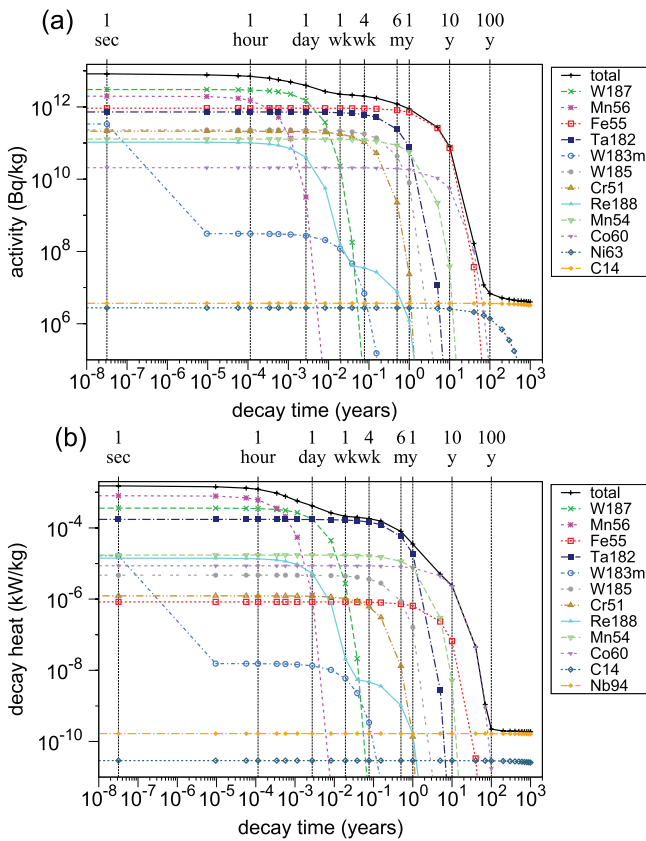
section 2.2) is the one present in the DEMO vessel at end-of-life (EOL), and is thus the most relevant for analysis of the decommissioning prospects, although we will consider the contributions from the earlier, removed divertors in the waste classification studies (section 3.3). As with the VV results in the previous section, there is very little change in this profile with time and so the time-evolution in the average activation response for the component is more informative, and is shown for all four DEMO-blanket concepts in figure 8.

Figure 7 demonstrates the expected variation, namely that cells more exposed to neutrons (rather than waste gases), which are those with the least amount (thickness) of material between them and the fusion plasma, become more activated than cells that are better shielded. In the figure, for example, cell 2 is producing the most activity and decay heat at 1 s and is almost directly exposed to neutrons from the plasma, with

only the armour and coolant layers for protection. On the other hand, the adjacent cells 1 and 3 are, on average, much less active due to the additional shielding—provided largely by cell 2.

The time evolution in average divertor body response (figure 8) shows that the activation is almost the same in each of the four DEMO-blanket concepts at all decay times, which is to be expected since the material and geometry of the divertor does not vary with concept.

While the activity and decay heat is initially higher in the divertor body than in the VV, which is probably unavoidable due to the higher neutron fluxes in the in-vessel regions, it is interesting to observe that at longer decay-times the reverse is true—the EUROFER steel of the divertor body is less active than the SS316 steel (compare figures 5 and 8), particularly at decay-timescales on the order of 100 years and beyond.



**Figure 9.** Radionuclide breakdown of the decay-profile of (a) activity, and (b) decay heat, averaged (by cell mass) across all divertor body cells in the HCPB concept.

Examining the time evolution in the component-averaged nuclide contributions for the divertor body of the HCPB concept (figure 9) reveals that the long-lived  $^{63}\text{Ni}$  isotope, which dominated the long-term activity of the VV (figure 6), is no longer important in EUROFER. This is due to the much lower concentration of Ni in the starting composition of EUROFER in comparison to SS316. The long-term activation in EUROFER is, instead, dominated by  $^{14}\text{C}$  in terms of absolute becquerel activity (figure 9(a)), while  $^{94}\text{Nb}$  is important for decay heat (figure 9(b)), although in both cases the levels of activity and decay heat are relatively tiny at these timescales. Both of these radionuclides could be reduced by changing the composition of EUROFER, either by element reduction or exchange, potentially improving the long-term activation characteristics of the steel even further. This could be particularly necessary to reduce  $^{14}\text{C}$ , as figure 9(a) suggests that it produces activity in the few  $\text{MBq kg}^{-1}$  range beyond 100 years, potentially influencing the reclassification of divertor components as low-level waste, which is determined by a  $\beta + \gamma$  activity limit of  $12 \text{ MBq kg}^{-1}$  (see section 3.3)— $^{14}\text{C}$  is a pure  $\beta$  emitter. Meanwhile,  $^{94}\text{Nb}$  produces significant  $\gamma$  dose, and so its production may have to be reduced in order to improve the recycling prospects of the divertor relative to the  $2 \text{ mSv h}^{-1}$  limit discussed in 3.3.

However, EUROFER does not have such a ‘low activation’ response at short decay times because of the 1.2 at.% W. Figure 9 shows that the  $^{187}\text{W}$  produced from W under

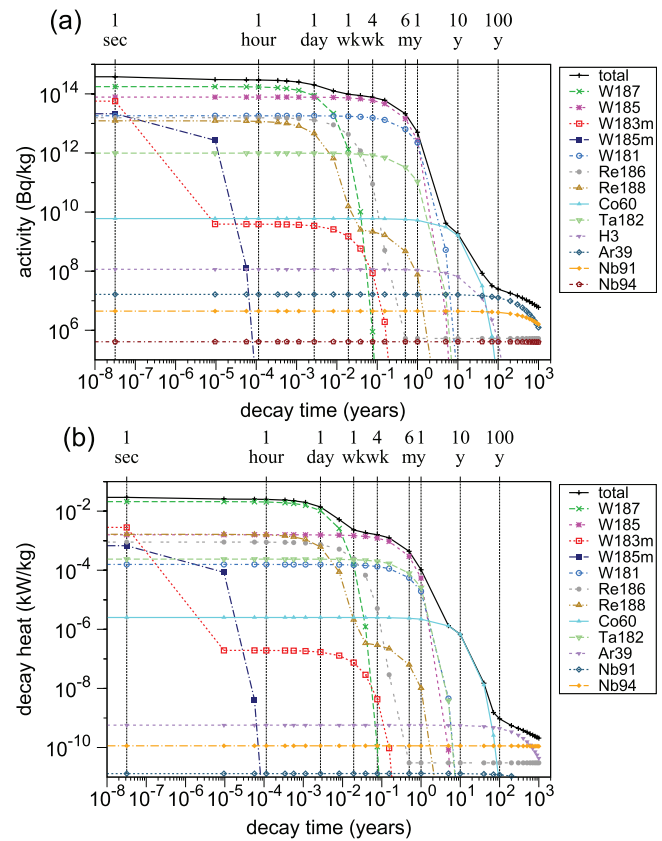


**Figure 10.** Radionuclide breakdown of the decay-profile of (a) activity, and (b) decay heat, averaged (by cell mass) across all final-replacement divertor armour cells in the HCPB concept.

irradiation causes significant activity, and to a lesser extent decay heat, during the first day after shutdown, which could have implications if immediate remote maintenance of the divertor is required.

**3.1.3. Divertor armour.** The armour layer of the divertor plasma-facing components (PFCs) is almost entirely W, and so the problem with short-term activity from  $^{187}\text{W}$  ( $T_{1/2} = 23.9 \text{ h}$ ) noted above for EUROFER is even more significant here. The component-averaged nuclide contributions to the activation of the divertor armour of the HCPB DEMO shown in figure 10 demonstrate the high activity and decay heat at short times caused predominantly by  $^{187}\text{W}$ —more than an order of magnitude greater than in the divertor body.

While the expected isotopes of W dominate the activity of the divertor armour at short timescales, it is interesting to note that at longer times, beyond around 10 years of decay, it is instead radionuclides produced from the minor impurities of the nominally pure W (99.96 wt.% W, but also containing 0.003% Fe, 0.01% Mo, 0.001% Co, 0.001% K, 0.001% Nb, 0.005% P, 0.002% Si, 0.003% C and several others) that contribute the majority of the activity. In particular, from figure 10,  $^{60}\text{Co}$  on the medium timescale, and then  $^{39}\text{Ar}$  ( $T_{1/2} = 269 \text{ years}$ ) at longer times with minor contributions at even longer times from isotopes of niobium. This potentially illustrates the need to pay more attention to the fabrication of W for near-plasma regions to reduce the concentration of the

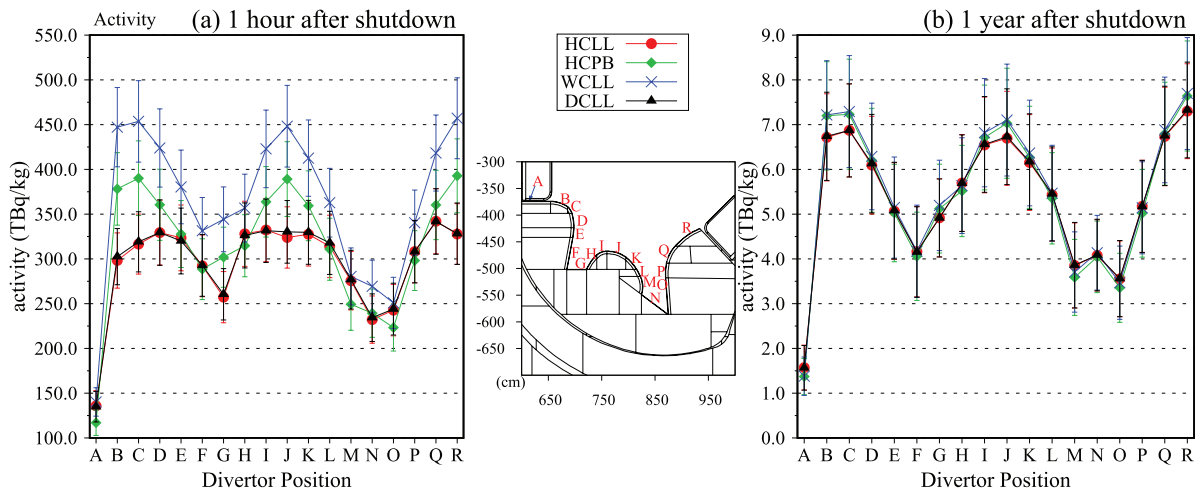


**Figure 11.** Poloidal variation in total activity in  $\text{TBq kg}^{-1}$  of the divertor armour (a) one hour, and (b) one year, after final DEMO shutdown. Results are shown for all four DEMO-blanket concepts. The toroidal cross section through the MCNP geometry indicates the position of the numbered divertor armour cells in the plots.

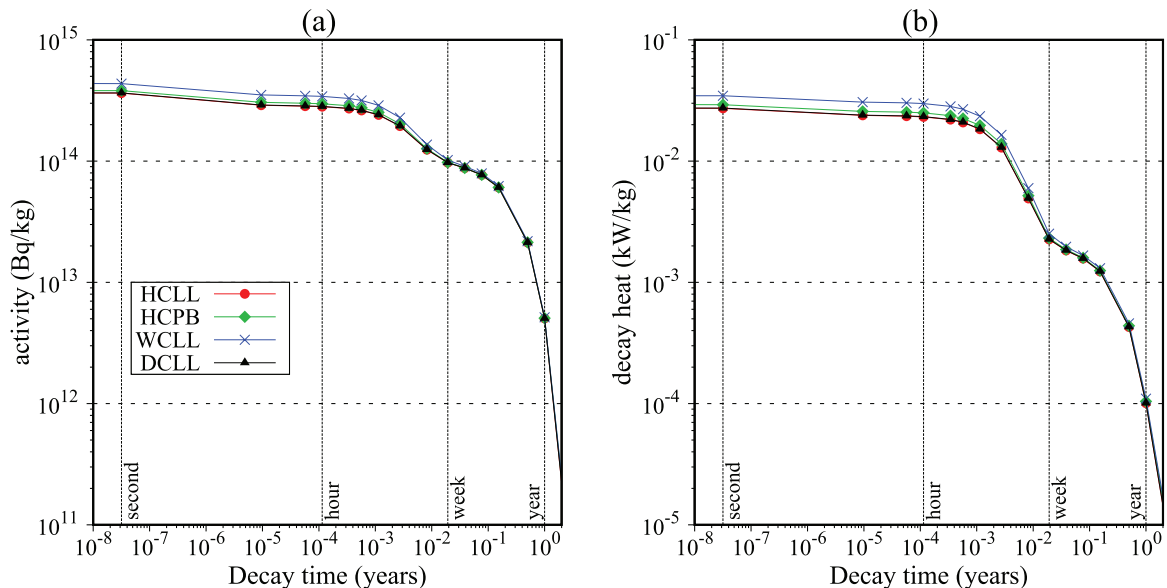


**Figure 12.** Decay profile of (a) activity, and (b) decay heat, averaged (by cell mass) across all divertor armour cells during the first 2 years following EOL.

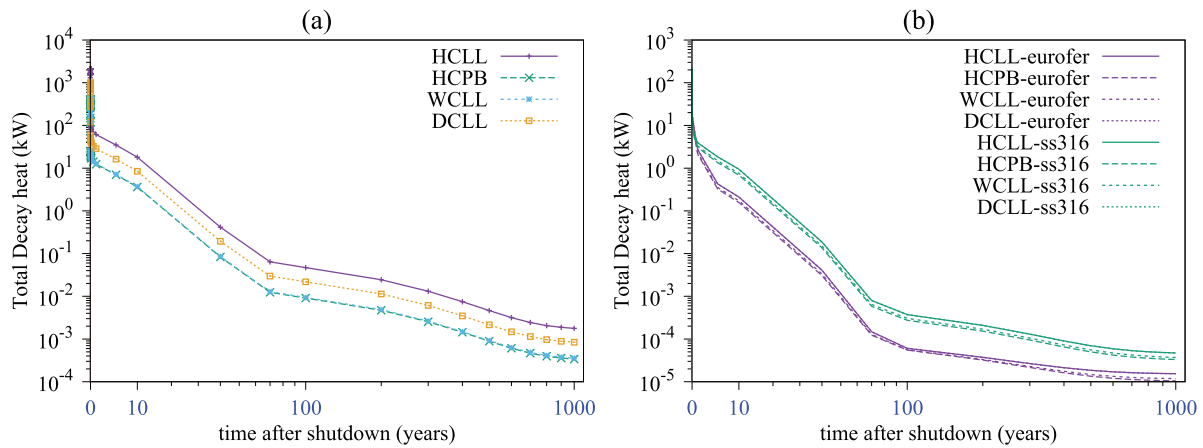
minor impurities (Fe, Co, K, Nb, Mo, etc) that produce these radionuclides.

Figure 11 shows the poloidal variation in activity in the divertor armour at two different decay times after DEMO shutdown. After 1 hour (figure 11(a)), there is a significant difference between the four DEMO-blanket concepts, particularly in the more exposed (to neutrons) cells such as B, J, and R. However, by 1 year after shutdown (figure 11(b)) the differences between the DEMO-blanket concepts have largely disappeared—as demonstrated in figure 12, where the component-averaged time-evolution curves for activity and decay heat in the different concepts can only be separated on timescales of less than around 1 week (the decay times in this plot have been truncated to 2 years to highlight this). This almost exactly agrees with the timescale of dominance for  $^{187}\text{W}$  in figure 10, which will be produced predominantly via  $(n,\gamma)$  reactions on  $^{186}\text{W}$  (28.43 atm.% of pure W) that are most

probable (have the highest reaction cross sections) at low neutron energies. The analysis suggests that the greater neutron moderation in the water cooled blanket of the WCLL concept results in neutron spectra with a higher proportion of low-energy neutrons in the divertor armour, thereby enhancing  $^{187}\text{W}$  production. This perfectly demonstrates how very subtle changes (in composition, neutron fields, etc) can have a significant influence on inventory results.

### 3.2. Total component decay heat

The total decay heat from a particular component is an important quantity to predict because, in particular, it will determine whether or not active cooling must be continued (and how long for) after DEMO has shutdown—a component cannot be allowed to heat-up beyond its design limit to prevent damage to itself and surrounding areas. The total decay heat



**Figure 13.** Total component decay heat predicted for (a) the entire VV, and (b) a single divertor cassette. Results are shown for all four DEMO-blanket concepts. Additionally, in (b), are results for a divertor cassette where the default EUROFER steel has been replaced by SS316.

from a particular cell can be obtained by multiplying the raw  $\text{kW kg}^{-1}$  from FISPACT-II by the cell's mass, and the total for a component by summing across all cells. For the VV total component decay heat profile in figure 13(a) this is equivalent to multiplying the component-average  $\text{kW kg}^{-1}$  in figure 5(b) by the total VV mass, including the scale-up to a full  $360^\circ$  Tokamak from the  $11.25^\circ$  sector used for the Monte-Carlo simulations. The divertor results in figure 13(b), on the other hand, is for all three layers of one divertor cassette occupying  $7.5^\circ$  of the Tokamak (there are 48 cassettes in the DEMO design considered here) and was calculated as two-thirds of the result obtained for the  $11.25^\circ$  model.

As seen in section 3.1.1, the HCLL concept is predicted to have the highest VV decay heat at all times after shutdown following the full DEMO operational schedule, with WCLL and HCPB the best performers (figure 13(a)). As a consequence, it might be necessary to continue with active cooling for longer in a HCLL DEMO reactor unless the shielding of the VV is greater compared to the other concepts. On the other hand, it is worth noting that the HCLL blanket modules themselves have the lowest decay heat during the first few days after shutdown [15].

The differences between concepts for the decay heat from a single divertor cassette (figure 13(b)) are naturally only minor. However, notice how the scale of the decay heat from a cassette is only around an order of magnitude less than that from the VV, despite there being more than two orders of magnitude difference in their respective masses—around 55 tonnes for a single divertor cassette in the present model (this is relatively high due to overestimated mixed-material densities— $\sim 15$  tonnes is more realistic), compared to almost 8000 tonnes of VV. This illustrates how active in-vessel components become, and suggests that a divertor cassette may need significant post-shutdown cooling, potentially even after it has been removed from the reactor.

Figure 13(b), includes a second set of decay-heat curves, this time for a cassette made predominantly from SS316 steel instead of EUROFER. These results were obtained by repeating the entire set of MCNP and FISPACT-II calculations for new versions of the DEMO model for each of the

four different blanket-concepts, where the EUROFER in the divertor-body cells had been replaced by the same SS316 used in the VV. The resulting total component decay heat for an SS316 divertor cassette in the figure is around a factor of 5 higher at all decay times greater than around 1 year (the differences are lower at shorter times), suggesting that such a divertor would require a longer period of active cooling following shutdown.

This difference is largely caused by the higher Co content in SS316 in comparison to EUROFER (0.05 versus 0.01 wt.%—see section 2.1), leading to the production of  $^{60}\text{Co}$ . This  $^{60}\text{Co}$  dominates the decay heat at timescales up to 100 years despite the relatively minor concentrations of Co in both steels, highlighting that small changes in composition can have a major impact on the radiological response.

### 3.3. Waste classification

Predicting the amount of waste produced from DEMO is vital to assess the likely environmental impact, which should be minimised, and disposal costs of DEMO, and also to secure regulatory approval. Using preliminary waste classifications (currently under review within Europe), based on UK regulations [16], for IAEA waste classes [17], it is possible to trace the time-evolution in waste masses in each class using the inventory output, both during operation and after shutdown. The mass of material (in fact 32 times the mass to account for a full  $360^\circ$ ) in every cell of the geometry (i.e. including all in-vessel and ex-vessel components present in the model, and the VV) was attributed to waste classes at each time-step using the following definitions and limits:

- **NAW— None Active Waste.** Material falls into this category if its IAEA clearance index [18] is at or below 1. Clearance index is a standard output per nuclide from FISPACT-II;
- **LLW— Low Level Waste.** Categorised as material with  $\alpha$  activity of less than  $4 \text{ MBq kg}^{-1}$  and a combined  $\beta + \gamma$  activity of less than  $12 \text{ MBq kg}^{-1}$ . FISPACT-II breaks-down the activity of each nuclide according to their

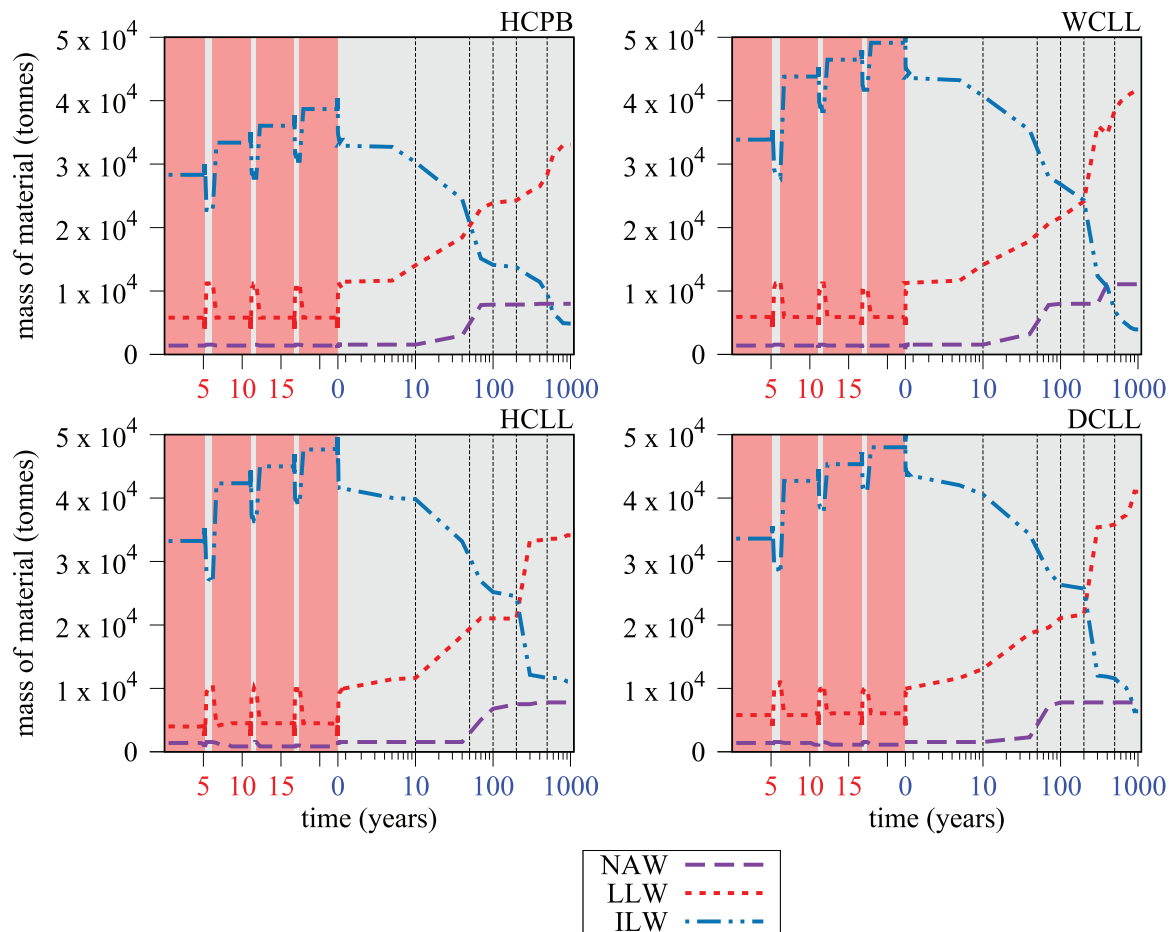


**Figure 14.** Time evolution in waste masses for the entire geometry of the four DEMO-reactor blanket concepts, including the main in-vessel components (blanket and divertor), the VV, and any ex-vessel regions that are present. The red regions in the plots indicate periods of operation and the grey regions represent shutdown and maintenance periods. The red time axis labels refer to the progression of the operational phase of DEMO plotted on a linear scale and the blue labels the EOL shutdown plotted on a logarithmic scale. To aid visualization, vertical gridlines are shown at 10, 50, 100, 200, and 500 years beyond EOL. See the main text for explanation of the waste abbreviations.

established decay schemes, making comparisons against these limits straightforward;

- ILW— Intermediate Level Waste. Material with activities above the LLW limits.

It was assumed that no waste fell into a further category for high level waste (HLW), which is based, additionally, on the cooling requirements of waste generating significant decay heat (this would most likely be arranged at a DEMO site and occur before material is released as waste). Where a component was replaced during operation, both the removed mass and its replacement were added to the appropriate waste class as a function of time—hence the need for the blank padding time-steps discussed in section 2.2. This means, for example, that the divertor results (figure 15) include the mass from four sets of divertor cassettes—each at different stages of decay at any given time.

In addition to the waste classifications there was also a preliminary assessment of the recyclability of components. As an approximate measure, a component was considered to be composed of potentially recyclable material (PRM) if the contact  $\gamma$  dose rate (calculated by FISPACT-II [8]) was below

$2 \text{ mSv h}^{-1}$ —a level below which the material could be manipulated by remote handling equipment without their electronics being too severely damaged (at least on the timescales necessary to perform the manipulation). Note that this limit is somewhat conservative, and more optimistic limits for advanced remote maintenance systems would use a much higher limit.

Figure 14 shows the evolution in waste masses (in tonnes) for the complete DEMO reactor in each of the four breeding-blanket concepts. In each of the plots the breakdown and growth of waste masses during the operation lifetime of 22.333 years is shown using a linear timescale, with red-background plasma-operation phases separated by grey maintenance periods for divertor and/or blanket replacement (see the inventory details in section 2.2). The subsequent end-of-life (EOL) decay out-to 1000 years is plotted on a logarithmic timescale. The figure clearly shows, in particular, the jumps in ILW and LLW waste masses associated with the additional divertor ( $\sim 2600$  tonnes per replacement) and blanket components when DEMO is restarted following the maintenance phases. It also demonstrates the lower overall masses associated with the HCPB concept because of the lower

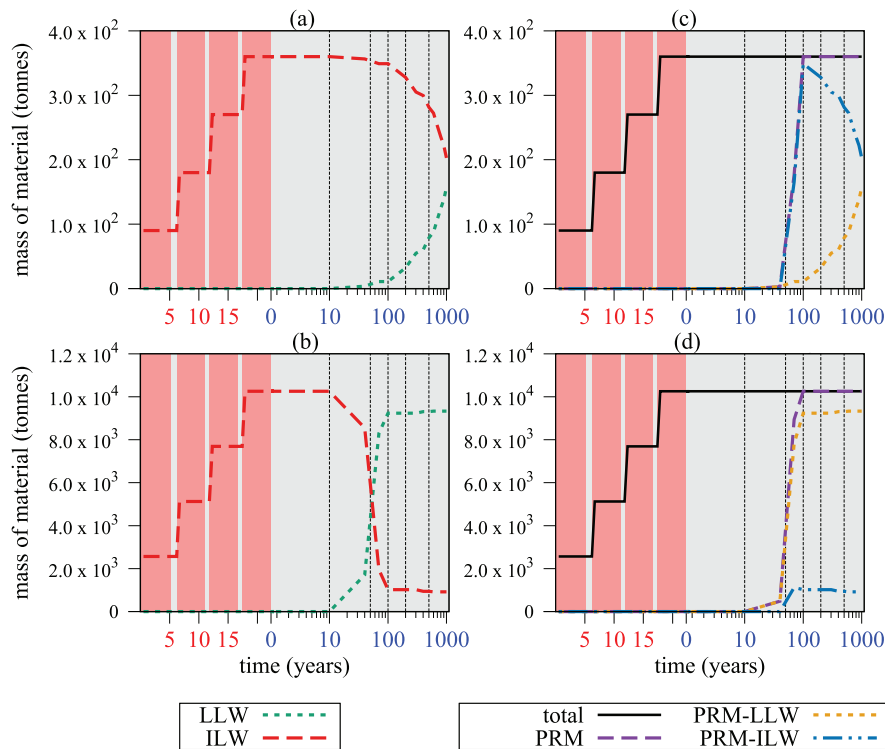


**Figure 15.** Time evolution in waste (a) and (b) and recyclable (c) and (d) masses for the HCPB divertor PFCs (a) and (c) and divertor body (b) and (d). The red regions in the plots indicate periods of operation and the grey regions represent shutdown and maintenance periods. The red time axis labels refer to the progression of the operational phase of DEMO plotted on a linear scale and the blue labels the decay following EOL shutdown plotted on a logarithmic scale. In (c) and (d), the total material mass is given and the recyclable material masses are additionally separated by waste class. To aid visualization, vertical gridlines are shown at 10, 50, 100, 200, and 500 years beyond EOL. See the main text for explanation of the abbreviations.

density of the blanket-module material in this ceramic pebble-bed concept ( $1.9 \text{ g cm}^{-3}$  for HCPB compared to an average of  $8.4 \text{ g cm}^{-3}$  for the three lithium-lead designs, resulting in total blanket masses of  $\sim 2400$ , and  $\sim 6500$  tonnes, respectively, per replacement). In particular, the HCPB concept has around 20% lower ILW mass at EOL, which is the classification of all blanket modules at this time, than any of the LiPb concepts. For comparison, the other major components include the VV with a total mass of 7600 tonnes, the Blanket manifold (not replaced) weighing 2400 tonnes, and the coils (toroidal and central solenoid) weighing 15 800 tonnes.

Most material of the DEMO model, including all of the VV and divertor, is ILW during operational lifetime and for the first few decades beyond EOL. A small fraction of the total mass never exceeds the LLW limits during operation (including some of the homogenized blanket modules), and during decay the LLW class grows until it eventually becomes the majority. The actual position of the cross-over between the ILW and LLW classes varies between the four DEMO-blanket concepts with HCPB performing better (having an earlier cross-over). The waste classification of the VV (not plotted separately) shows the differences between the models even more clearly, although in no concept does the VV become significantly LLW until several hundred years after shutdown. For HCLL this situation is particularly bad, with virtually none of the VV classifiable as LLW, even after 1000 years, demonstrating again the potential issue with the HCLL concept. However, the VV cells used in the present DEMO model

are relatively thick, with homogenized materials and density. A more detailed analysis, with heterogeneous VV cells, would be expected to produce a gradient of neutron fluxes across the VV—instead of just a single value,—leading to a different distribution across the waste classes. Indeed, ongoing studies [14] for a VV split into 10 layers (with depth), suggest that the waste analysis could be more favourable, with the VV behind the HCPB concept becoming 50% LLW after around 200 years (compared to around 500 years in the present work). These results will be the subject of future publications. Increased heterogeneity would also alter the results for some of the in-vessel components, particularly the blanket modules.

Finally, in figure 14, for all four blanket concepts, little of the waste mass is classifiable as NAW until it has been decay-cooling for more than 50 years, and none of the VV becomes NAW at any time. Figure 15, which shows the waste and recycling classification results for the HCPB divertor body and PFCs (results for other DEMO-blanket concepts are predictably indistinguishable from this), shows that there is also no NAW mass for the divertor, which is not surprising for an in-vessel component exposed to significant neutron fluxes. Indeed, all of the NAW mass classified in this analysis originates from ex-vessel port or coil components.

The HCPB waste analysis for the divertor PFCs in figure 15(a), and for the divertor body in figure 15(b), both show that virtually all of the waste mass is ILW at shutdown, and that the divertor PFCs remain largely ILW even after 1000 years of decay. Note that the divertor PFCs include both the W

armour discussed in section 3.1.3 and the cooling layer, containing CuCrZr, Cu and water, beneath it. The long-lived  $^{63}\text{Ni}$  ( $T_{1/2} = 100.6$  years), produced via  $(n, p)$  reactions on  $^{63}\text{Cu}$  (the main isotope of Cu at 69.17 atm.%), is the reason why the divertor PFCs remain significantly ILW at such long decay times. For the divertor body, on the other hand, in figure 15(b), the waste is predicted to decay enough to become almost entirely LLW between around 10 and 100 years, which is exactly the timescale over which  $^{55}\text{Fe}$  and  $^{60}\text{Co}$  decay away (see figure 9).

However, despite the differences in the waste analysis of the divertor PFCs and body, the recycling-mass estimates in figures 15(c) and (d), respectively, show similar results. In both cases the components are predicted to become potentially recyclable within 100 years. For the VV the situation is the same, with the entire mass of SS316 steel PRM within 100 years.

#### 4. Summary

Extensive neutron-transport and inventory simulations have been performed for a DEMO model with different tritium breeding blanket concepts in identical reactor geometries. The resulting predictions have been used to assess and compare the activation and decay-heat of the vacuum vessel (VV) and divertor of the European DEMO design after the expected operational lifetime. Additionally, the waste production prospects of the reactor geometry have been investigated using a preliminary classification system based on IAEA and UK guidelines.

In the fixed geometry of the model, which was optimised for the helium-cooled pebble-bed (HCPB) option, the helium-cooled lithium-lead (HCLL) blanket modules provide significantly less shielding, leading to greater activation in the VV. This suggests that, for the present DEMO design, the HCLL (and to a lesser extent the dual-cooled lithium-lead, DCLL) blanket concept would require additional design-optimisation to achieve the same neutron-shield protection as provided by either the HCPB or WCLL concepts. At the same time, the subtle changes in the neutron fields produced by the different blanket concepts can also have localized impact on in-vessel components, for example, causing higher short-lived activity in the divertor armour near the WCLL blanket modules.

Component-averaged radionuclide inventories, which are similar for all four blanket concepts, for the plasma-facing armour of the divertor suggest that the minor impurities present in the manufacturing specifications of 'pure' W create long-lived activation products, indicating the need for careful control of material compositions. Meanwhile, in the EUROFER steel of the divertor and the SS316 steel of the VV, the usual short-lived radionuclides ( $^{55}\text{Fe}$ ,  $^{56}\text{Mn}$ ) dominate at short decay-timescales. However, at longer times there are noticeable variations caused by subtle differences in the compositions of the steels, and SS316 performs badly, producing not only more  $^{60}\text{Co}$  than EUROFER, but also long-lived nuclides of Ni. As a consequence, using SS316 as the structural steel in a divertor cassette is predicted to cause five times more decay

heat post-operation than an equivalent cassette constructed of EUROFER (the default).

Waste classification predictions, which included all components modelled in the geometry (blanket modules, VV, divertor, and some ex-vessel components), indicate that the majority of the DEMO vessel, but particularly the steel of the VV and divertor, will remain as intermediate level waste (ILW) for many decades (or even centuries) after shutdown before decaying sufficiently to allow reclassification as low level waste (LLW). However, neither the VV or in-vessel components (blanket and divertor) decay sufficiently in 1000 years to satisfy the IAEA clearance index limit for none active waste (NAW), and the tungsten armour of the divertor remains largely ILW on this timescale. After around 100 years, the VV and divertor are predicted to be recyclable for all DEMO reactor designs. Note that the homogenization across the thickness of the VV in the present DEMO model significantly overestimates the activity of outer VV regions (far from the plasma), while underestimating inner regions. This could significantly alter the predictions made here, and so an analysis of a more realistic, heterogeneous VV is part of ongoing work.

#### Acknowledgments

This work has been carried out within the framework of the EUROfusion Consortium and has received funding from the Euratom research and training programme 2014–2018 under grant agreement No 633053 and from the RCUK energy programme (grant number EP/I501045). To obtain further information on the data and models underlying this paper please contact [PublicationsManager@ccfe.ac.uk](mailto:PublicationsManager@ccfe.ac.uk). The views and opinions expressed herein do not necessarily reflect those of the European commission.

#### References

- [1] Pelowitz D.B. (ed) 2013 *MCNP6 User Manual, Version 1.0* Los Alamos (document number: LA-CP-13-00634, Rev. 0. Further details at <http://mcnp.lanl.gov/>)
- [2] Villari R. 2014 Neutron shielding study of the DEMO upper vertical port *Report No. 2APSUF*, EUROfusion
- [3] Federici G., Biel W., Gilbert M.R., Kemp R., Taylor N. and Wenninger R. 2017 *Nucl. Fusion* accepted
- [4] Bachmann C. et al 2015 *Fusion Eng. Des.* **98–9** 1423–6
- [5] Fischer U., Bachmann C., Palermo I., Pereslavitsev P. and Villari R. 2015 *Fusion Eng. Des.* **98–9** 2134–7
- [6] Federici G. et al 2014 *Fusion Eng. Des.* **89** 882–9
- [7] Davis A. and Turner A. 2011 *Fusion Eng. Des.* **86** 2698–700
- [8] Sublet J.C., Eastwood J.W., Morgan J.G., Fleming M. and Gilbert M.R. 2016 The FISPACT-II User Manual CCFE-R(11) 11 Issue 8, (CCFE) (<http://fispect.ukaea.uk>)
- [9] López Aldama D. and Trkov A. 2012 FENDL-2.1: update of an evaluated nuclear data library for fusion applications *Report No. INDC(NDS)-467*, IAEA ([www-nds.iaea.org/publications/indc/indc-nds-0467/](http://www-nds.iaea.org/publications/indc/indc-nds-0467/))
- [10] Chadwick M.B. et al 2011 *Nucl. Data Sheets* **112** 2887–996 (Special Issue on ENDF/B-VII.1 Library. See also <http://t2.lanl.gov/nis/data/endl/>)
- [11] Gilbert M.R., Zheng S., Kemp R., Packer L.W., Dudarev S.L. and Sublet J.C. 2014 *Fusion Sci. Tech.* **66** 9–17

- [12] Sublet J.C., Packer L.W., Kopecky J., Forrest R.A., Koning A.J. and Rochman D.A. 2010 The European activation file: EAF-2010 neutron-induced cross section library, CCFE-R(10)05 (Available from [www.ccf.ac.uk/EASY2007.aspx](http://www.ccf.ac.uk/EASY2007.aspx))
- [13] Harman J. 2012 DEMO operational concept description *Report No. 2LCY7A*, EUROfusion/EFDA
- [14] Gilbert M.R. and Eade T. 2016 Assessment of activation contact dose rate of IVCs and vessel *Report No. 2M7WD2*, EUROfusion
- [15] Eade T., Travleev A., Pereslavytsev P., Stankunas G., Sanz J., Garcia R., García M. and Ogando F. 2016 Activation and decay heat analysis of the European DEMO blanket concepts *29th Symp. on Fusion Technology (Prague, Czech Republic, 5–9 September 2016)* (<http://www.soft2016.eu/>)
- [16] Strategy for the management of solid low level radioactive waste from the non-nuclear industry in the United Kingdom, Department of Energy & Climate Change, UK 2012 (Available at [www.gov.uk/government/publications/](http://www.gov.uk/government/publications/))
- [17] IAEA Safety Standards 2009 *Classification of Radioactive Waste (General Safety Guide vol GSG-1)* (Vienna: IAEA) ([www-pub.iaea.org/MTCD/publications/PDF/Pub1419\\_web.pdf](http://www-pub.iaea.org/MTCD/publications/PDF/Pub1419_web.pdf))
- [18] IAEA 1996 *Clearance Levels for Radionuclides in Solid Materials: application of the Exemption Principles* (Vienna: IAEA) IAEA-TECDOC-855 [www-pub.iaea.org/MTCD/publications/PDF/Pub1202\\_web.pdf](http://www-pub.iaea.org/MTCD/publications/PDF/Pub1202_web.pdf)